2013

Carbon nanotube and boron nitride nanotube hosted C_{60}–V nanopeapods

Guiling Zhang
Harbin University of Science and Technology

Rulong Zhou
Hefei University of Technology

Xiao Cheng Zeng
University of Nebraska-Lincoln, xzeng1@unl.edu

Journal of Materials Chemistry C

Materials for optical and electronic devices

www.rsc.org/MaterialsC

Volume 1 | Number 30 | 14 August 2013 | Pages 4507–4606

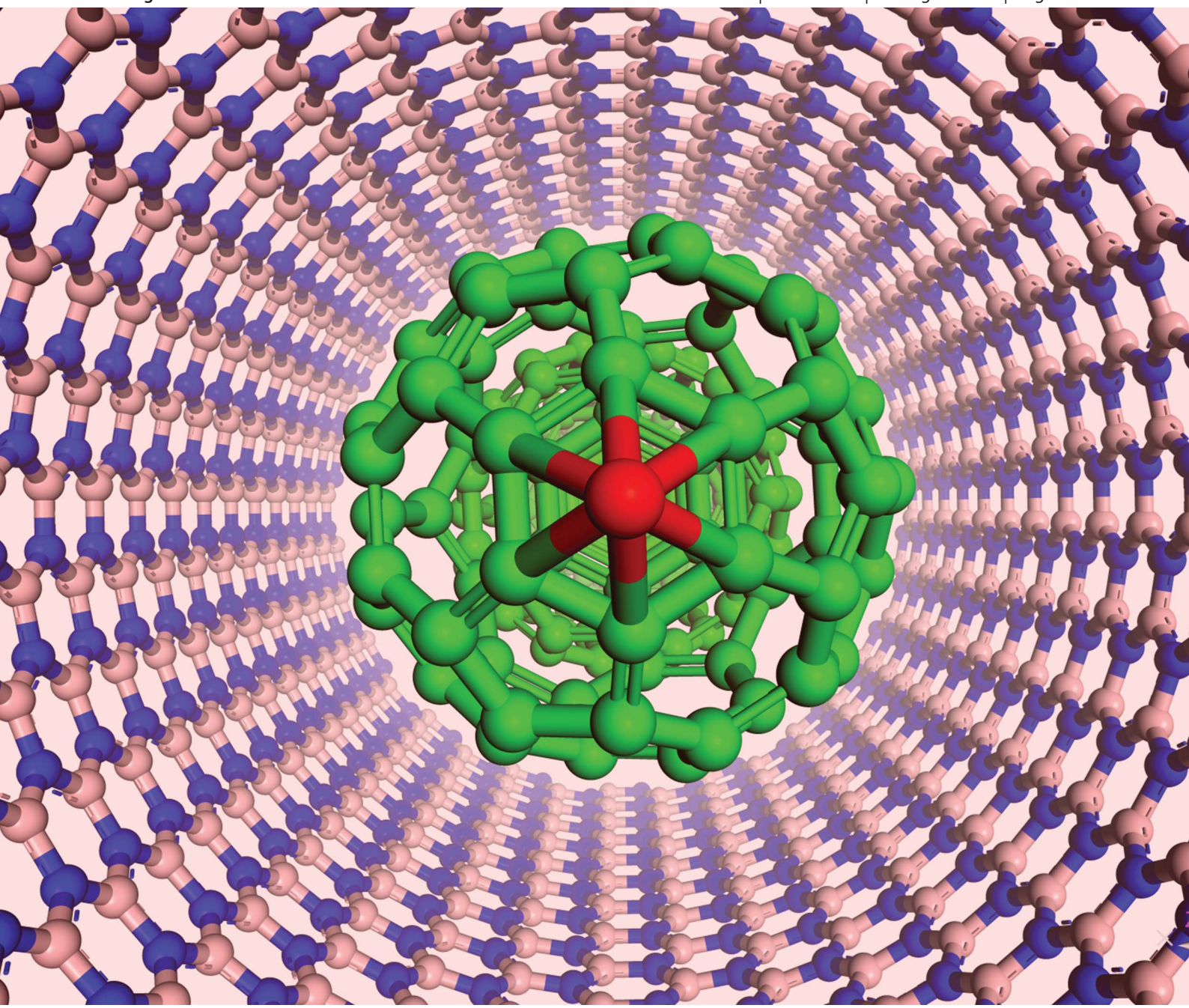

ISSN 2050-7526

RSC Publishing

PAPER

Xiao Cheng Zeng *et al.*

Carbon nanotube and boron nitride nanotube hosted C_{60}–V nanopeapods

2050-7526(2013)1:30;1-G

Journal of Materials Chemistry C

RSC Publishing

PAPER

View Article Online
View Journal | View Issue

Carbon nanotube and boron nitride nanotube hosted C_{60}–V nanopeapods†

Cite this: *J. Mater. Chem. C*, 2013, **1**, 4518

Guiling Zhang,[ac] Rulong Zhou[bc] and Xiao Cheng Zeng*[c]

We investigate electronic and transport properties of a novel form of nanopeapod structure, where the "pod" component is either a carbon nanotube (CNT) or a boron-nitride nanotube (BNNT) while the "pea" component is a chain of C_{60}–V dimers. Compared to the conventional carbon peapod where the "pea" is a chain of C_{60} fullerenes, marked changes in the electronic structures are found due to the formation of coordination bonds between V and two neighboring C_{60} molecules. The local spins in the (η^6-C_{60}–V)@CNT or (η^6-C_{60}–V)@BNNT peapod are coupled *via* antiferromagnetic (AFM) exchange interaction. In particular, the C_{60}–V chain in BNNT yields a well-defined spin qubit. Density-functional theory calculation suggests that the (η^6-C_{60}–V)@CNT peapod is metallic with characteristics of multiple carriers contributed from CNTs, C_{60}, and V. The (η^6-C_{60}–V)@BNNT peapod is predicted to be semiconducting with a narrow band gap, and its charge carriers are contributed by the C_{60}–V chain. Evidently, the insertion of a V atom between every two C_{60} fullerenes can enhance the conductivity of the peapod. Binding H atoms on all the α positions of the pentagons in C_{60} can further strengthen the V–C_{60} interaction. Both AFM and FM states of the H-containing peapod are nearly degenerate in energy. The FM state gives rise to a magnetic moment of 3.0 μ_B per unit cell, three times greater than that of the V–benzene or V–cyclopentadiene multidecker complexes. The binding of H atoms to the C_{60} however cannot enhance electron transport due to the removal of the π channel of C_{60}. Previous experiments have demonstrated that C_{60} molecules can enter BNNTs through the open tips of the BNNTs, offering a strategy that the V–C_{60} dimers may be encapsulated into nanotubes through the open tips of the nanotubes to form M–C_{60} peapods.

Received 28th April 2013
Accepted 25th May 2013

DOI: 10.1039/c3tc30800f

www.rsc.org/MaterialsC

Introduction

Nanopeapods, nanotubes (NT) filled with fullerene molecules (C_n@NT), have attracted intensive interest due to their potential applications in field-effect transistors,[1–3] magnetic nanodevices,[4–7] data storage nanodevices,[8,9] and nanoscale lasers.[10] Being trapped in the cylindrical interior of nanotubes, the fullerene molecules may form a one-dimensional (1D) wire structure. In contrast to the 1D structure assembled on a substrate, the confined 1D structure within a nanotube exhibits exceptional thermal stability owing to the spatial protection by the host nanotube.[11] This hybrid core/sheath structure enables the development of a novel class of 1D nanostructures unavailable in open environment. Moreover, the electronic coupling between various components, including fullerene–nanotube and fullerene–fullerene, may lead to new physical phenomena that cannot be observed with isolated nanotubes and fullerenes. For example, recent scanning tunneling microscopy (STM) imaging on the carbon nanotube (CNT) peapod, C_{60}@CNT, shows the modulation of density of states (DOS) in the conduction band with the same period as the 1D C_{60} array,[12,13] which can affect the electron transport property of the CNT.[14–17]

CNT peapods have been successfully synthesized in many laboratories.[18] The first evidence of C_{60} nested inside carbon nanotubes was reported in 1998.[19] Later, higher fullerenes, *e.g.* C_{70},[20,21] C_{80},[20] and C_{84},[22] endohedral fullerenes, *e.g.* Gd@C_{82},[23,24] PrSc@C_{84},[25] and N@C_{60},[26,27] and other modified fullerenes, *e.g.* C_{59}N (ref. 28) and C_{59}R (R = alkyl),[29] were also experimentally detected inside CNTs. Theoretical computations have yielded additional details of the energetics,[30,31] electronic structures,[30–36] and transport properties[37–39] of CNT peapods. However, few studies have reported boron–nitrogen nanotube (BNNT) peapods. Note that BNNTs were first reported by Okada *et al.* in 2001.[40] Soon after, this nanomaterial was fabricated in the laboratory by Mickelson *et al.*[41] Since then, structural and electronic properties of BNNT peapods have been explored theoretically.[42,43] The BNNT peapods can be viewed as a single-file fullerene chain, where the fullerene molecules are confined to form a linear chain

[a]*Key Laboratory of Green Chemical Engineering and Technology of College of Heilongjiang Province, College of Chemical and Environmental Engineering, Harbin University of Science and Technology, Harbin 150040, China*

[b]*School of Science and Engineering of Materials, Hefei University of Technology, Hefei, Anhui, 230009, China*

[c]*Department of Chemistry, University of Nebraska-Lincoln, Lincoln, NE 68588, USA*

† Electronic supplementary information (ESI) available. See DOI: 10.1039/c3tc30800f

which interacts with the BNNT host through weak van der Waals interaction.[42] It is known that the CNTs can be either metallic or semiconducting, depending on their diameter and chirality, while the BNNTs are always insulating with band gaps of 4–5 eV.[44–47] Such a striking difference in electronic properties between CNTs and BNNTs will inevitably lead to different physical properties of the corresponding peapods. For the CNT peapods, there are two conducting pathways: one along the CNTs and the other along the encapsulated fullerene chain.[30] However, for the BNNT peapods, the electron transport is expected to be only through the fullerene t_{1u}-derived bands.[42]

A possible experimental strategy to endow either CNT or BNNT peapods with new properties is to encage exohedral or endohedral fullerenes. Recently, fullerene derivatives containing transition metal atoms adsorbed on the outer surface of the carbon cage have received increasing interest because such complexes can possess properties of transition metals and fullerenes.[48–51] It is known that transition metal (TM) atoms can be coordinated with benzenes (η^6-type) or cyclopentadienes (η^5-type) and form 1D sandwich multidecker clusters. However, it is still a challenge to synthesize η^6- and η^5-type transition metal–fullerene complexes due to the curved surface of fullerene and associated weak polarizability.[48–51] Here, the superscript of η denotes the number of carbon atoms that are bonded to a metal atom. Two research groups have synthesized both neutral and cationic clusters, η^6-$M_n(C_{60})_m$ and η^6-$M_n(C_{60})_m^+$ (M = Sc, Ti, V, Cr, Fe, Ni, Ag; m and n are integers).[52,53] Only small-sized clusters ($n \leq 4$) were proposed to form a stable multi-pod structure in the gas-phase. For large-sized clusters ($n > 4$), the TM–fullerene complexes favor either a multiple dumbbell or a ring configuration. Hence, it is unlikely to fabricate a long-chain of M–C_{60} multi-pods due to multiple facets of fullerenes, as each facet can coordinate with a transition metal atom. On the other hand, the nanotube can be a perfect cylindrical host to enclose a 1D M–C_{60} multi-pod nanowire. In addition, previous diffraction measurements[54–57] and high resolution transmission electron microscopy (HRTEM) imaging[54–57] show that the distance between the C_{60} molecules within nanotubes almost always falls into the range of 9.7–10.0 Å, a sufficient interval for inserting a transition metal atom to form M–C_{60} multi-pod complexes. Furthermore, both experimental and theoretical studies have demonstrated that exohedral functional groups (*e.g.* –H and –Me) of fullerenes can also stabilize the M–fullerene complexes.[49,50] Various transition metal–fullerene complexes, *e.g.*, $Re(\eta^5\text{-}C_{60}H_5)(CO)_3$ (ref. 58) and $(\eta^5\text{-}C_5H_5)MC_{60}R_5$ (M = Fe, Ru, R = Me, Ph),[59] have already been successfully encapsulated into CNTs. Based on the aforementioned results and our calculations, we expect that 1D M–C_{60} peapods in either CNT or BNNT may be realized in the laboratory.

In this work, we compute properties of eight V-containing CNT peapods **1a–1h** and eight V-containing BNNT peapods **2a–2h** at different spin states (Fig. 1 and ESI Fig. S1†) using the density functional theory (DFT) method. For the host nanotubes, we consider the metallic (10,10) CNT and the insulating (10,10) BNNT. The transition metal element V is selected in view

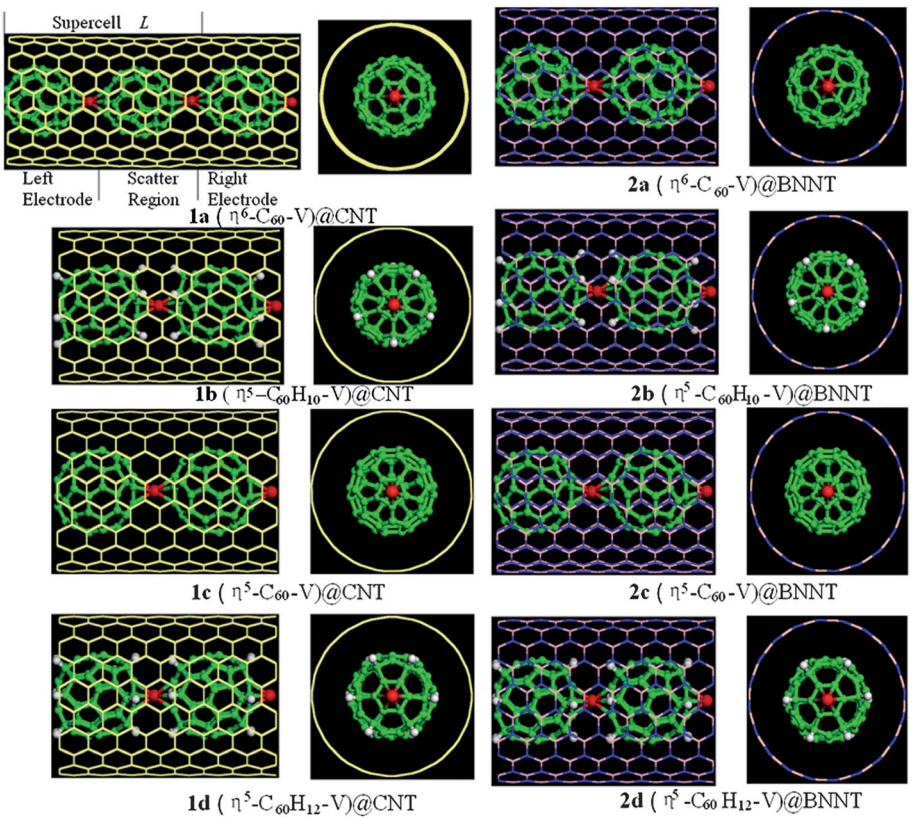

Fig. 1 Optimized multi-pod structures of V-containing peapods, **1a–d** and **2a–d**. **1a** also illustrates a two-probe system for electron transport calculation. The most stable structures **1a**, **2a**, **1b**, and **2b** are discussed in this text.

of the fact that most benzene and cyclopentadiene sandwich multideckers are V complexes. The (10,10) nanotube and C_{60} fullerene are chosen because they have been subjected to extensive studies both theoretically and experimentally.[34] For the purpose of comparison, we also compute properties of the V-free C_{60}@CNT and C_{60}@BNNT peapods. In particular, the electronic and transport properties of the two most stable CNT peapods **1a** and **1b** and the two most stable BNNT peapods **2a** and **2b** are discussed in detail. Particular attention is placed on the effects of the V element on the electronic and transport properties of the peapods, as well as the effects of the attachment of H atoms to the C_{60}, and the difference between the CNT and BNNT peapods.

Results and discussion

We use a supercell containing two repeated units (*i.e.*, containing two C_{60}s and two V atoms; see **1a** in Fig. 1) in the axial direction to account for the magnetic exchange interaction due to the presence of the V element.

Favorable location for V binding

We first consider the systems without H (**1a**, **2a**, **1c** and **2c** in Fig. 1, **1e–h** and **2e–h** in the ESI Fig. S1†). To confirm that the favorable location for the V atom is just between the C_{60}s (sandwich multi-pod structure, **1a**, **2a**, **1c**, and **2c**), we also optimize peapods with every V atom being located in the space between the tube and the C_{60} (ESI Fig. S1†). These side-V-binding structures can be divided into two groups: (1) the pVh structure, if the V atom is located between a pentagon of C_{60} and a hexagon of nanotube, and (2) the hVh structure if the V atom is between a hexagon of C_{60} and a hexagon of nanotube (ESI Fig. S1†). For the pVh and hVh structures, all the *cis* and *trans* structures of **1e–h** and **2e–h** are examined. In the *cis* structure, the V atoms are aligned on the same side of the C_{60}s along the axial direction, while in the *trans* structure the V atoms are located alternatively on the opposite side of the C_{60}s along the axial direction. Both the antiferromagnetic state (AFM) and the ferromagnetic state (FM) are examined for the eight CNT peapods **1a–h** and eight BNNT peapods **2a–h**. The computed total energies E per supercell are listed in the ESI Table S1.† Note that all the sandwich multi-pod structures possess lower energies than the corresponding side-V-binding structures, indicating that the V atom favors to be located between C_{60}s and link the fullerenes to form a 1D V–C_{60} hybrid multi-pod chain within either CNT or BNNT. Clearly, the hybrid multi-pod structure of the η^6-type (C_{60}–V)@NT is more stable than that of the η^5-type one (**1a** *vs.* **1c** and **2a** *vs.* **2c**). Time of flight mass spectroscopy measurements[52,53] and *ab initio* calculation[60] also confirm that the C_{60} behaves as a η^6-ligand for the V atom. Therefore, the η^6-type hybrid multi-pod structures **1a** and **2a** are energetically most favorable for the peapods (without H), which will be discussed in the following sections.

The chemical stability for the V-binding with peapods (without H) is evaluated by computing the reaction energy per supercell for the net reaction [nanotube (NT) + $2C_{60}$ + 2V → peapod − ΔE_r]. The computed reaction energies for all peapods are listed in the ESI Table S1.† As a comparison, the reaction energies of V-free C_{60}@NT peapods (based on the reaction [NT + $2C_{60}$ → peapod − ΔE_r]) are also given in the ESI Table S1.† The ΔE_r of C_{60}@CNTs are in the range of −6.66 to −6.92 eV, in agreement with the experimental value of −6.0 eV.[61] Importantly, the V-free C_{60}@NT multipods prefer a pentagon-facing-pentagon (denoted as pfp) configuration for C_{60}s rather than a hexagon-facing-hexagon (hfh) configuration. The formation of the V-containing structures releases 16–20 eV energies per supercell, much more than the V-free ones, implying that incorporation of the V atom into either C_{60}@CNT or C_{60}@BNNT is energetically favorable.

Next, we examine reaction energies of two types of H-containing peapods, (η^5-$C_{60}H_{10}$–V)@NT (**1b** and **2b**) and (η^6-$C_{60}H_{12}$–V)@NT (**1d** and **2d**). Similarly, the reaction energy ΔE_r per supercell is computed through the reaction formula [NT + $2C_{60}H_{12}$/$2C_{60}H_{10}$ + 2V → peapod − ΔE_r]. The computed reaction energies for the H-containing peapods are given in the ESI Table S1.† Apparently, the attachment of the H atoms in the manner described above is more exothermic for the C_{60}–V binding reaction. This is because with the H atoms attaching two opposing pentagons or hexagons of a C_{60} (forming $C_{60}H_{10}$ or $C_{60}H_{12}$), a structure of the cyclopentadiene type or a benzene type is formed. These exohedral H atoms can modify the local structure of the molecular orbitals. As a result, a favorable condition arises to the formation of the complex of the fullerene with the V atom through the η^5- or η^6-type bond. The formation of (η^5-$C_{60}H_{10}$–V)@NT gives rise to more negative ΔE_r than the formation of (η^6-$C_{60}H_{12}$–V)@NT, suggesting that the η^5-H-substitution is energetically more favorable for binding with V atoms. Hereafter, for H-containing multi-pods, only the η^5-H-substituted **1b** and **2b** systems will be discussed.

Geometric structures and chemical bonding

The optimized supercell length in the axial direction (L) (**1a** in Fig. 1), the face-to-face distances between adjacent fullerenes (r), and the distances between the wall of the nanotube and the nearest atom of C_{60} (R) of **1a**, **2a**, **1b**, and **2b** are given in Table 1. The distances r are within the range of 3.43–3.64 Å, similar to the ligand-to-ligand separation in the V–benzene (3.3–3.4 Å)[62] or V–cyclopentadiene (3.54 Å)[63] multidecker clusters. The C_{60}s in BNNT have a slightly longer separation than in CNT. The values of R are in the range of 3.30–3.49 Å, suggesting a van der Waals interaction between the CNT and the fullerene. There are no major geometry differences between the AFM and FM states of the four V-containing systems. No significant structural change is observed with the V doping except slight elongation of the r, indicating that the V atom can be sandwiched between C_{60}s without deforming either the nanotube or the C_{60} structure. Therefore, the formation of the 1D V–C_{60} multi-pod chain would not require much structural distortion from the original V-free peapod.

Table 2 shows the charge populations in the peapods **1a**, **2a**, **1b**, and **2b**. About 1.2 electrons move from the V 4s orbital to the fullerene cage, while about 2.0 C_{60} electrons move to the empty V 3d and 4p orbitals, indicative of a typical V-cage coordination bond. Overall, a V atom bears a net negative charge. The V–C_{60}

Table 1 Calculation results for V–C_{60} peapods **1a**, **2a**, **1b**, and **2b**.[a] Those for V-free C_{60}@CNT(PP) and C_{60}@BNNT(PP) are listed for comparison

Peapods	$\Delta E_{r,\,AFM}/\Delta E_{r,\,FM}$ (eV)	ΔE_{FM-AFM} (meV)	J (meV)	$T_{C(N)}$ (K)	S_{AFM}/S_{FM} (μ_B)	S_{FM}^{V} (μ_B)	$S_{FM}^{C_{60}}$ (μ_B)	L_{AFM}/L_{FM} (Å)	r_{AFM}/r_{FM} (Å)	R_{AFM}/R_{FM} (Å)
1a (η^6-C_{60}–V)@CN	−18.54/−18.44	107.06	107.1	414	0.0/2.0	1.0	0.0	19.88/19.98	3.43/3.43	3.30/3.33
2a (η^6-C_{60}–V)@BNNT	−18.44/−18.36	80.32	80.3	311	0.0/2.2	1.1	0.0	20.08/20.08	3.49/3.52	3.40/3.39
1b (η^5-$C_{60}H_{10}$–V)@CNT	−26.68/−26.68	3.62	3.6	28	0.0/6.0	2.5	0.5	19.92/19.92	3.59/3.59	3.38/3.38
2b (η^5-$C_{60}H_{10}$–V)@BNNT	−26.46/−26.46	2.38	2.4	19	0.0/6.0	2.3	0.7	20.14/20.12	3.63/3.64	3.47/3.49
C_{60}@CNT(pfp)	−6.92	—	—	—	0.0	0.0	0.0	19.86	3.33	3.34
C_{60}@BNNT(pfp)	−6.78	—	—	—	0.0	0.0	0.0	20.08	3.32	3.42

[a] For peapods with antiferromagnetic (AFM) and ferromagnetic (FM) states: the reaction energy per supercell (ΔE_r), the energy difference per supercell between FM and AFM states (ΔE_{FM-AFM}), the exchange parameter per supercell (J), the Curie or Neél temperature ($T_{C(N)}$), the total magnetic moment per supercell (S), the local magnetic moment on the V atom (S_{FM}^{V}) and C_{60} ($S_{FM}^{C_{60}}$), respectively, the supercell parameter along the axial direction (L), the nearest face-to-face distance between adjacent fullerenes (r), and the distance between the wall of the nanotube and the nearest atom of C_{60} (R).

Table 2 Charge populations in V–C_{60} peapods **1a**, **2a**, **1b**, and **2b**. Those for V-free C_{60}@CNT(pfp) and C_{60}@BNNT(pfp) are listed for comparison

Peapods	q^{NT}	$q^{C_{60}}$	$q^{C_{60}H_{10}}$	q^{V}	$q^{V(4s)}$	$q^{V(3d+4p)}$
1a (η^6-C_{60}–V)@CNT	0.10	0.82	—	−0.92	1.19	−2.11
2a (η^6-C_{60}–V)@BNNT	−0.43	1.27	—	−0.84	1.21	−2.05
1b (η^5-$C_{60}H_{10}$–V)@CNT (AFM)	0.13	—	0.52	−0.64	1.26	−1.90
1b (η^5-$C_{60}H_{10}$–V)@CNT (FM)	0.12	—	0.52	−0.64	1.26	−1.90
2b (η^5-$C_{60}H_{10}$–V)@BNNT (AFM)	−0.42	—	1.04	−0.62	1.27	−1.89
2b (η^5-$C_{60}H_{10}$–V)@BNNT (FM)	−0.42	—	1.04	−0.62	1.27	−1.88
C_{60}@CNT(pfp)	0.11	−0.11	—	—	—	—
C_{60}@BNNT(pfp)	−0.43	0.43	—	—	—	—

interaction can be also reflected from the projected density of states (PDOS) shown in Fig. 2. The 3d state of the V atom hybrids significantly with the π states of the fullerene. The Kohn–Sham orbitals corresponding to the energy levels near the Fermi level (E_f) at the Γ point for **1a**, **2a**, **1b**, and **2b** are shown in Fig. 3, where it clearly shows the hybridization of the V 3d and fullerene π orbitals. In the carbon nanotube peapods **1a** and **1b**, the CNTs exhibit positive charges and thus the fullerene cages serve as the electron acceptor (Table 2). This conclusion is consistent with previous theoretical calculations.[30,33,38] Conversely, the BNNT is an electron acceptor for the peapods **2a** and **2b**. The encapsulation of the V atoms and the addition of the H atoms have little effect on the charge transfer between the nanotube and the fullerene.

Magnetism

The calculated energy differences between the AFM and FM states are listed in Table 1 and ESI Table S1.† Besides GGA calculation, the GGA + U calculation (see Computational methods) is also performed to confirm no appreciable change in the magnetic moments (see ESI Table S1†). The (η^6-C_{60}–V)@CNT and (η^6-C_{60}–V)@BNNT peapods possess the AFM ground state with zero magnetic moment, in contrast to the FM ground state in the V–benzene or V–cyclopentadiene multidecker nanowire.[63–65] This apparent difference in magnetic behavior may be attributed to the difference in the interaction between the 3d electrons of the V atom and the π electrons of the carbon rings; the d–π interaction is discontinuous in the peapod (⋯d–π–π–d–π–π⋯ bonding type), but is continuous in the V–benzene and V–cyclopentadiene multidecker nanowires (⋯d–π–d–π⋯ bonding type). In other words, each unit cell of (η^6-C_{60}–V)@NT has a spin ½, and the neighboring unpaired electron is antiferromagnetically coupled due to the exchange interaction of the intervening C_{60}. In (η^6-C_{60}–V)@BNNT, the spin moment is mainly contributed by C_{60}–V. As shown in Fig. 3, both valence band maximum (VBM) and

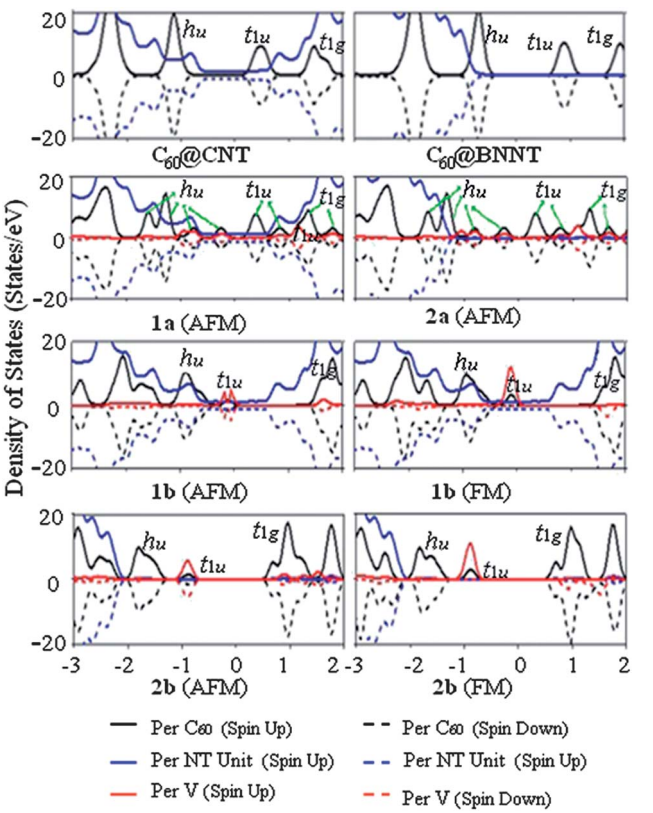

Fig. 2 Computed projected density of states (PDOS) of **1a**, **2a**, **1b**, and **2b** peapods.

conduction band minimum (CBM) of (η^6-C_{60}–V)@BNNT can be attributed to the coupling of the V 3d and C_{60} π orbitals. The C_{60}–V chain in **2a** gives rise to a 0.43 eV band gap at the Γ point (Fig. 3). Therefore, the (η^6-C_{60}–V)@BNNT valence band is well separated from other energy bands above and below, leading to a well-defined spin qubit. However, in (η^6-C_{60}–V)@CNT, the energy band due to C_{60}–V crosses with other bands due to CNTs and thus cannot form an effective spin qubit.

The exchange parameter J, which can be estimated by the energy difference between FM and AFM configurations, is over 60 meV per supercell (containing two spins). The values of J calculated for (η^6-C_{60}–V)@NT peapods (>80 meV) as shown in Table 1, are much larger than those of the endohedral fullerene Sc@C_{82} peapods (<17 meV).[66] We also estimate the Curie or Neél temperatures, $T_{C(N)}$, of the peapods using the formula $3/2k_BT_{C(N)} = J/2$ (see Table 1). The estimated Curie or Neél temperatures of (η^6-C_{60}–V)@CNT and (η^6-C_{60}–V)@BNNT are higher than 300 K, suggesting that the AFM state of the (η^6-C_{60}–V)@NT peapod may be thermally stable at room temperature.

It is worth noting that the AFM and FM states of the H-substituted system, either (η^5-$C_{60}H_{10}$–V)@CNT or (η^5-$C_{60}H_{10}$–V)@BNNT, are nearly degenerate in energy. The binding of five H atoms to the C_{60} leads to the formation of a radical of the cyclopentadienyl type. In the FM state, the unpaired electrons of the H-substituted $C_{60}H_{10}$ are coupled with the 3d electrons of the V atom. Consequently, the FM state shows a magnetic moment $S > 2.0$ μ_B per V atom and $S < 1.0$ μ_B per $C_{60}H_{10}$, giving rise to a total $S = 6.0$ μ_B per supercell (*i.e.*, $S = 3.0$ μ_B per unit cell), three times larger than that of the V–benzene or V–cyclopentadiene multidecker complex. The magnetic behavior of the AFM and FM states is reflected in the projected density of states (PDOS) shown in Fig. 2. For the AFM states, the majority spin and the minority spin are nearly the same near the Fermi level so that their net magnetic moments are nearly zero. For the FM

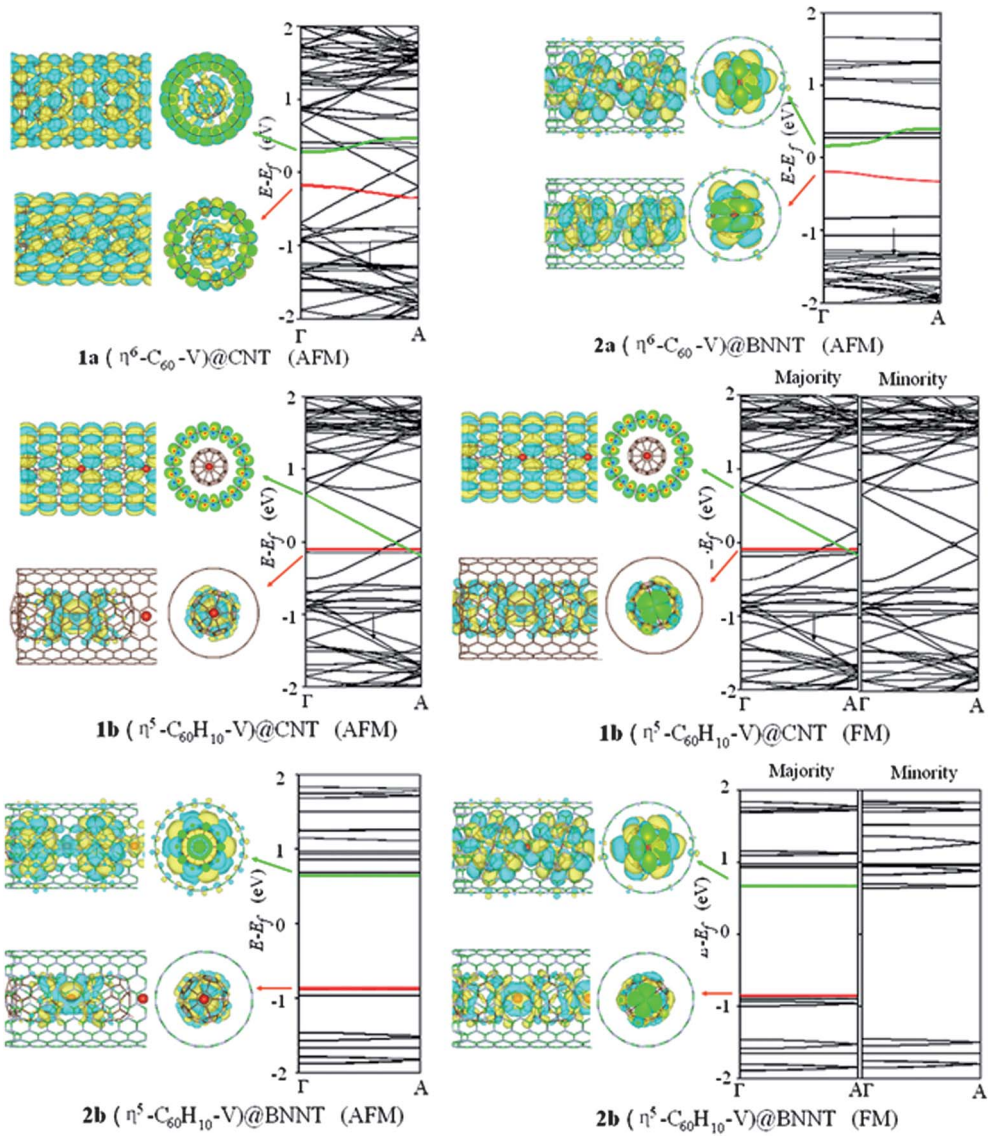

Fig. 3 Computed band structures (right panels) of **1a**, **2a**, **1b**, and **2b** peapods and the Kohn–Sham orbitals (left and middle panels) corresponding to the energy levels (highlighted in red and/or green lines) near E_f at Γ point. The value of the iso-surface is 0.05 (e Å^{-3}).

state, the majority spin below the Fermi level is greater than the minority spin. The spin polarization is mainly due to the V atoms. These novel magnetic properties of the H-substituted (η^5-$C_{60}H_{10}$–V)@CNT and (η^5-$C_{60}H_{10}$–V)@BNNT peapods may have potential applications for magnetic nanodevices.

Transport property

Fig. 3 plots the band structures of **1a**, **2a**, **1b**, and **2b**. For the purpose of comparison, the band structures of the V-free C_{60}@CNT and C_{60}@BNNT peapods are given in the ESI Fig. S2.† For the C_{60}@CNT peapod, two bands cross the Fermi level (E_f) with large and linear dispersion, retaining the character of the π orbitals of the CNT. Hence, the C_{60}@CNT is a metal. The flat h_u and t_{1u} bands originated from the π orbitals of C_{60} and lie within the valence and the conduction bands, as clearly seen from the PDOS (Fig. 2). This is different from an earlier study that the t_{1u} bands of C_{60} also cross the Fermi level.[13] In that study, the lattice parameter was constrained to be 9.824 Å and the band structures were computed based on the local-density approximation (LDA), while in this study a full geometry optimization is performed based on the spin-polarized generalized gradient approximation (GGA). Note that a topographic STM image of the C_{60}@CNT(17,0) also shows that the t_{1u} state of C_{60} corresponds to the conduction band.[32] From the PDOS, one can see that only the π states of the CNT make a contribution at the Fermi level. The fullerene h_u (∼−1.2 eV), t_{1u} (∼0.4 eV), and t_{1g} (∼1.4 eV) states hybridize with the π states of the CNT to different extent. This result is consistent with the STM study of the C_{60} peapods.[12,13] Therefore, the fullerene π states can also participate in the electron tunneling through the CNT. As such, the encaging of C_{60} by the CNT should enhance the electronic conduction of the CNT, consistent with a previous experimental measurement.[17] For the C_{60}@BNNT peapod, the top valence band and bottom conduction band are contributed solely by the C_{60} h_u and t_{1u} states, respectively, suggesting that the transport would be primarily through the C_{60}. The C_{60}@BNNT peapod is predicted to be a semiconductor with a band gap ∼1.35 eV, close to the reported value of 1.2 eV.[42]

Next, for the V-containing systems **1a**, **2a**, **1b**, and **2b**, marked changes in electronic structures can be seen from Fig. 2 and 3. For the non-H systems **1a** and **2a**, the coupling between the 3d state of the V atom and the π states of the fullerene leads to the splitting of the h_u, t_{1u}, and t_{1g} states (Fig. 2). A new band originated from the hybridization of the V 3d state and the C_{60} h_u state appears just below the Fermi level (Fig. 3), indicating that the doping of V atoms increase the number of quantum channels. This new band also enhances the π state coupling between the C_{60} and the CNT in (η^6-C_{60}–V)@CNT near E_f, but has little influence on the π interaction between the C_{60} and the BNNT in (η^6-C_{60}–V)@BNNT. The (η^6-C_{60}–V)@CNT peapod is a metal with characters of multiple carriers stemming from the CNT, C_{60}s, and V atoms. The plotted Kohn–Sham orbitals in Fig. 3 demonstrate a feature of multiple carriers for the (η^6-C_{60}–V)@CNT peapod. For the (η^6-C_{60}–V)@BNNT peapod, the coupling between the C_{60} and the V atom results in a remarkable downshift of the fullerene t_{1u} conduction band closer to the Fermi level, and a narrow band gap

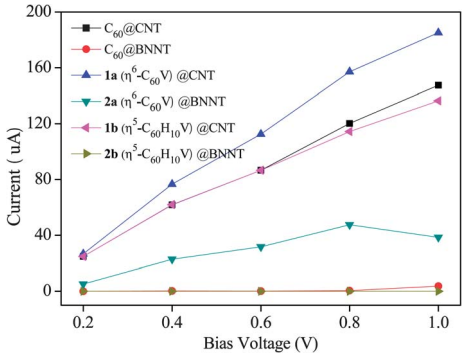

Fig. 4 The calculated *I*–*V* curves of **1a**, **2a**, **1b**, and **2b**. For comparison, the *I*–*V* curves for C_{60}@CNT and C_{60}@BNNT are also presented.

(0.43 eV). The charge carriers are distributed on both fullerene and V atom (Fig. 2 and 3).

For the H-substituted peapods **1b** and **2b**, the H-fullerene chain also shows h_u-, t_{1u}-, and t_{1g}-like states near the Fermi level. From Fig. 2 and 3, it is found that the t_{1u}-like states of the $C_{60}H_{10}$ are downshifted to the top of the valence band and coupled with the V 3d states for both (η^5-$C_{60}H_{10}$–V)@CNT and (η^5-$C_{60}H_{10}$–V)@BNNT peapods, suggesting more electron carriers than the multidecker chain. However, the (η^5-$C_{60}H_{10}$–V)@BNNT system has a larger band gap (1.53 eV) than the non-H substituted system (1.35 eV), due to the weakening of the π delocalization of the fullerene by the –H attachment.

To confirm the predication of the transport property based on the electronic structures, we have also computed transport properties of finite-sized **1a**, **2a**, **1b**, and **2b** between two electrodes. Three transport behaviors are seen from Fig. 4 and 5: (1) the C_{60}@CNT peapod shows a metal character while the C_{60}@BNNT peapod shows an insulating one, proving that the metallic CNT severs as the main transport channel for C_{60}@CNT, and the C_{60} chain is the main channel for C_{60}@BNNT. (2) The current in the case of V-containing peapod is greater than that of the corresponding non-V system [(η^6-C_{60}–V)@CNT *vs.* C_{60}@CNT and (η^6-C_{60}–V)@BNNT *vs.* C_{60}@BNNT], indicating that the incorporation of V atoms can enhance the conductivity. The V atoms clearly contribute to the transport of the (η^6-C_{60}–V)@CNT and (η^6-C_{60}–V)@BNNT peapods. (3) The

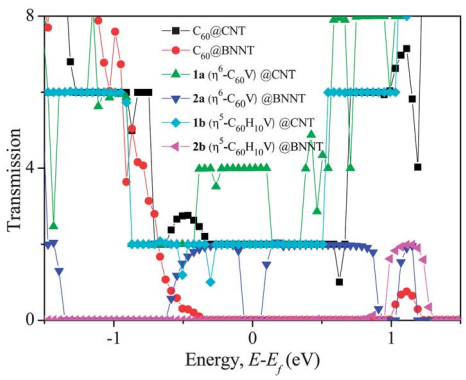

Fig. 5 Transmission spectra of **1a**, **2a**, **1b**, and **2b**. For comparison, transmission spectra for C_{60}@CNT and C_{60}@BNNT are also given.

attachment of H atoms to the C_{60} indeed weakens the electron transport [(η^6-C_{60}–V)@CNT *vs.* (η^6-$C_{60}H_{10}$–V)@CNT and (η^6-C_{60}–V)@BNNT *vs.* (η^6-$C_{60}H_{10}$–V)@BNNT]. The transmission around the Fermi level for (η^6-$C_{60}H_{10}$–V)@CNT arises only from the CNT, that is, no contribution from the $C_{60}H_{10}$–V chain owing to the weakening of the C_{60} π channel by the H attachment. All these transport characteristics are consistent with those derived from band structure analysis.

Conclusions

We have investigated the electronic and transport properties of a novel form of V–C_{60} peapods by means of density functional theory methods. It is found that the dopant V atoms tend to be located between neighboring fullerene cages along the axial direction. The spins in (η^6-C_{60}–V)@CNT and (η^6-C_{60}–V)@BNNT are coupled *via* antiferromagnetic exchange interactions, and the C_{60}–V chain in (η^6-C_{60}–V)@BNNT provides a well-defined spin qubit. The (η^6-C_{60}–V)@CNT peapod is a metal with characters of multiple carriers due to the nanotube, enclosed fullerenes and V atoms. The (η^6-C_{60}–V)@BNNT possesses a narrow band gap (0.43 eV) with charge carriers distributed on fullerenes and V atoms. With the V atoms located sandwiched between C_{60}s, the electron transport of the peapod can be enhanced. Binding hydrogen atoms to the α position with respect to the pentagons of C_{60} can strengthen the V–fullerene interaction. The AFM and FM states of the H-substituted systems, (η^5-$C_{60}H_{10}$–V)@CNT and (η^5-$C_{60}H_{10}$–V)@BNNT, are nearly iso-energetic. The FM state shows a total magnetic moment $S = 6.0$ μ_B per supercell ($S = 3.0$ μ_B per unit cell), three times higher than that of the V–benzene and V–cyclopentadiene multidecker complexes. The attachment of H atoms to the C_{60}, however, weakens the electron transport due to the weakening of the π channel of C_{60}s. Finally, we note that previous experiments have demonstrated that C_{60} molecules can enter BNNTs through the open ends of the BNNTs,[41] offering a strategy that the C_{60} transition-metal (M–C_{60}) dimers may be encapsulated into nanotubes through the open ends of the nanotubes to form M–C_{60} peapods. In addition to V,[73] we expect other transition metals such as M = Ti, Fe, and Mn might be in place of V to give rise to different magnetic or transport properties.[74]

Computational methods

Geometry optimizations are carried out using a linear combination of the atomic orbital method and density-functional theory, implemented in SIESTA 3.0 package.[67] The spin-polarized generalized gradient approximation (GGA) in Perdew–Burke–Ernzerhof (PBE) form together with the split valence double-ζ basis sets plus polarization (DZP) are selected for the DFT calculations.[68] A real-space grid with an equivalent energy cutoff of 200 Ry is adopted to expand the electron density for numerical integration. The core corrections are included for generating the corresponding pseudopotentials. Nonrelativistic and relativistic norm-conserving pseudopotentials generated in the Troullier–Martins scheme[69,70] are used for H, B, C, N, and V, respectively. The electronic configuration of $3p^6 3d^3 4s^2$ is used to refer to the valence state of V. The supercell dimensions in the x and y directions are set to be 32 Å, large enough to neglect interactions among periodic images of the nanotubes. Only the Γ point is adopted for the k-point sampling. Electron transport properties of the peapods are computed using the TRANSIESTA program in the SIESTA 3.0 pakage.[71] The two electrodes are selected to be the same as the scattering part in the TRANSIESTA calculation (Fig. 1). The single-zeta plus polarization (SZP) basis set is selected to reduce high computing cost associated with the computation of transport properties.

To ensure that the predicted relative stability for V binding based on the SIESTA package is reliable, we also perform a cross-checking calculation for peapods **1a–d** and **2a–d** using the VASP package. The PW91 functional and the projector augmented wave (PAW) method are selected. In addition, the on-site correlation effects among 3d electrons of the V atom are accounted for by using the GGA + U scheme,[72] where the parameter U–J is set to be 3. The plane-wave basis set cutoff is 400 eV. Spin-polarized calculations are performed for all peapod structures. Only the Γ point is chosen for the k-point sampling. As shown in the ESI Table S1,† the predicted chemical stabilities based on the reaction energies for various structures are consistent with the SIESTA calculations.

Acknowledgements

GLZ is supported by grants from the NSFC (51073048), the NSF of Heilongjiang Province of China (B201102), the science foundation for leaders in academy of Harbin City of China (2010RFJGG016, 2013RFXXJ024), and the science foundation for Outstanding Scientists of Harbin University of Science and Technology. XCZ is supported by grants from the NSF (EPS-1010674) and ARL (W911NF1020099), and by the University of Nebraska's Holland Computing Center.

References

1 T. Shimada, T. Okazaki, R. Taniguchi, T. Sugai, H. Shinohara, K. Suenaga, Y. Ohno, S. Mizuno, S. Kishimoto and T. Mizutani, *Appl. Phys. Lett.*, 2002, **81**, 4067–4069.
2 H. Y. Yu, D. S. Lee, S. H. Lee, S. S. Kim, S. W. Lee, Y. W. Park, U. Dettlaff-Weglikowska and S. Roth, *Appl. Phys. Lett.*, 2005, **87**, 163118.
3 Y. F. Li, T. Kaneko and R. Hatakeyama, *Nanotechnology*, 2008, **19**, 415201.
4 S. C. Benjamin, A. Ardavan, G. A. D. Briggs, D. A. Britz, D. Gunlycke, J. Jefferson, M. A. G. Jones, D. F. Leigh, B. W. Lovett, A. N. Khlobystov, S. A. Lyon, J. J. L. Morton, K. Porfyrakis, M. R. Sambrook and A. M. Tyryshkin, *J. Phys.: Condens. Matter*, 2006, **18**, S867–S883.
5 F. Simon, H. Kuzmany, B. Náfrádi, T. Fehér, L. Forró, F. Fülöp, A. Jánossy, L. Korecz, A. Rockenbauer, F. Hauke and A. Hirsch, *Phys. Rev. Lett.*, 2006, **97**, 136801.
6 F. Simon, *J. Nanosci. Nanotechnol.*, 2007, **7**, 1197–1220.
7 S. Tóth, D. Quintavalle, B. Náfrádi, L. Forró, L. Korecz, A. Rockenbauer, T. Kálai, K. Hideg and F. Simon, *Phys. Status Solidi B*, 2008, **245**, 2034–2037.

8 Y.-K. Kwon, D. Tománek and S. Iijima, *Phys. Rev. Lett.*, 1999, **82**, 1470–1473.
9 J. W. Kang and H. J. Hwang, *Mater. Sci. Eng.*, 2005, **C25**, 843–847.
10 S. L. He and J. Q. Shen, *Chin. Phys. Lett.*, 2006, **23**, 211–213.
11 O. Dubay and G. Kresse, *Phys. Rev. B: Condens. Matter Mater. Phys.*, 2004, **70**, 165424.
12 D. J. Hornbaker, S.-J. Kahng, S. Misra, B. W. Smith, A. T. Johnson, E. J. Mele, D. E. Luzzi and A. Yazdani, *Science*, 2002, **295**, 828–831.
13 S. Okada, M. Otani and A. Oshiyama, *Phys. Rev. B: Condens. Matter Mater. Phys.*, 2003, **67**, 205411.
14 P. W. Chiu, S. F. Yang, S. H. Yang, G. Gu and S. Roth, *Appl. Phys. A*, 2003, **76**, 463–467.
15 P. Utko, J. Nygård, M. Monthioux and L. Noé, *Appl. Phys. Lett.*, 2006, **89**, 233118.
16 Y. F. Li, T. Kaneko and R. Hatakeyama, *Appl. Phys. Lett.*, 2008, **92**, 183115.
17 A. Eliasen, J. Paaske, K. Flensberg, S. Smerat, M. Leijnse, M. R. Wegewijs, H. I. Jørgensen, M. Monthioux and J. Nygård, *Phys. Rev. B: Condens. Matter Mater. Phys.*, 2010, **81**, 155431.
18 A. N. Khlobystov, D. A. Britz and G. A. D. Briggs, *Acc. Chem. Res.*, 2005, **38**, 901–909.
19 B. W. Smith, M. Monthioux and D. E. Luzzi, *Nature*, 1998, **396**, 323–324.
20 K. Hirahara, S. Bandow, K. Suenaga, H. Kato, T. Okazaki, H. Shinohara and S. Iijima, *Phys. Rev. B: Condens. Matter Mater. Phys.*, 2001, **64**, 115420.
21 A. Guo, Y. Fu, J. Liu, L. Guan, Z. Shi, Z. Gu, R. Huang and X. Zhang, *J. Phys. Chem. B*, 2006, **110**, 9923–9926.
22 H. Kataura, Y. Maniwa, T. Kodama, K. Kikuchi, K. Hirahara, K. Suenaga, S. Iijima, S. Suzuki, Y. Achiba and W. Krätschmer, *Synth. Met.*, 2001, **121**, 1195–1196.
23 J. Lee, H. Kim, S. J. Kahng, G. Kim, Y. W. Son, J. Ihm, H. Kato, Z. W. Wang, T. Okazaki, H. Shinohara and Y. Kuk, *Nature*, 2002, **415**, 1005–1008.
24 T. Okazaki, T. Shimada, K. Suenaga, Y. Ohno, T. Mizutani, J. Lee, Y. Kuk and H. Shinohara, *Appl. Phys. A*, 2003, **76**, 475–478.
25 R. J. Nicholls, K. Sader, J. H. Warner, S. R. Plant, K. Porfyrakis, P. D. Nellist, G. A. D. Briggs and D. J. H. Cockayne, *ACS Nano*, 2010, **4**, 3943–3948.
26 K. Hirahara, K. Suenaga, S. Bandow, H. Kato, T. Okazaki, H. Shinohara and S. Iijima, *Phys. Rev. Lett.*, 2000, **85**, 5384–5387.
27 F. Simon, H. Kuzmany, H. Rauf, T. Pichler, J. Bernardi, H. Peterlik, L. Korecz, F. Fülöp and A. Jánossy, *Chem. Phys. Lett.*, 2004, **383**, 362–367.
28 G. Pagona, G. Rotas, A. N. Khlobystov, T. W. Chamberlain, K. Porfyrakis and N. Tagmatarchis, *J. Am. Chem. Soc.*, 2008, **130**, 6062–6063.
29 T. W. Chamberlain, A. Camenisch, N. R. Champness, G. A. D. Briggs, S. C. Benjamin, A. Ardavan and A. N. Khlobystov, *J. Am. Chem. Soc.*, 2007, **129**, 8609–8614.
30 S. Okada, S. Saito and A. Oshiyama, *Phys. Rev. Lett.*, 2001, **86**, 3835–3838.
31 M. Otani, S. Okada and A. Oshiyama, *Phys. Rev. B: Condens. Matter Mater. Phys.*, 2003, **68**, 125424.
32 Y. Cho, S. Han, G. Kim, H. Lee and J. Ihm, *Phys. Rev. Lett.*, 2003, **90**, 106402.
33 M.-H. Du and H.-P. Cheng, *Phys. Rev. B: Condens. Matter Mater. Phys.*, 2003, **68**, 113402.
34 M. Melle-Franco, H. Kuzmany and F. Zerbetto, *J. Phys. Chem. B*, 2003, **107**, 6986–6990.
35 J. Lu, S. Nagase, S. Zhang and L. Peng, *Phys. Rev. B: Condens. Matter Mater. Phys.*, 2003, **68**, 121402.
36 L. Ge, J. H. Jefferson, B. Montanari, N. M. Harrison, D. G. Pettifor and G. A. D. Briggs, *ACS Nano*, 2009, **3**, 1069–1076.
37 H. Kondo, H. Kino and T. Ohno, *Phys. Rev. B: Condens. Matter Mater. Phys.*, 2005, **71**, 115413.
38 J. Lu, S. Nagase, S. Re, X. Zhang, D. Yu, J. Zhang, R. Han, Z. Gao, H. Ye, S. Zhang and L. Peng, *Phys. Rev. B: Condens. Matter Mater. Phys.*, 2005, **71**, 235417.
39 S. Ni, W. He, Z. Li and J. Yang, *J. Phys. Chem. C*, 2011, **115**, 12760–12762.
40 S. Okada, S. Saito and A. Oshiyama, *Phys. Rev. B: Condens. Matter Mater. Phys.*, 2001, **64**, 201303.
41 W. Mickelson, S. Aloni, W. Han, J. Cumings and A. Zettl, *Science*, 2003, **300**, 467–469.
42 V. Timoshevskii and M. Côté, *Phys. Rev. B: Condens. Matter Mater. Phys.*, 2009, **80**, 235418.
43 Y. F. Li, H. Q. Yu, H. Li, K. Zhang, C. G. An, K. M. Liew and X. F. Liu, *J. Phys. Chem. C*, 2010, **114**, 11421–11424.
44 A. Rubio, J. L. Corkill and M. L. Cohen, *Phys. Rev. B: Condens. Matter Mater. Phys.*, 1994, **49**, 5081–5084.
45 X. Blase, A. Rubio, S. G. Louie and M. L. Cohen, *Europhys. Lett.*, 1994, **28**, 335–340.
46 J. Cumings and A. Zettl, *Chem. Phys. Lett.*, 2000, **316**, 211–216.
47 W. Q. Han, W. Mickelson, J. Cumings and A. Zettl, *Appl. Phys. Lett.*, 2002, **81**, 1110–1112.
48 S.-K. Goh and D. S. Marynick, *J. Comput. Chem.*, 2001, **22**, 1881–1886.
49 E. Nakamura, *Pure Appl. Chem.*, 2003, **75**, 427–434.
50 E. G. Gal'pern, A. R. Sabirov and I. V. Stankevich, *Phys. Solid State*, 2007, **49**, 2330–2334.
51 B. Molina, L. Pérez-Manriquez and R. Salcedo, *Molecules*, 2011, **16**, 4652–4659.
52 A. Nakajima, S. Nagao, H. Takeda, T. Kurikawa and K. Kaya, *J. Chem. Phys.*, 1997, **107**, 6491–6494.
53 S. Nagao, T. Kurikawa, K. Miyajima, A. Nakajima and K. Kaya, *J. Phys. Chem. A*, 1998, **102**, 4495–4500.
54 K. Hirahara, S. Bandow, K. Suenaga, H. Kata, T. Okazaki, H. Shinohara and S. Iijima, *Phys. Rev. B: Condens. Matter Mater. Phys.*, 2001, **64**, 115420.
55 H. Kataura, Y. Maniwa, M. Abe, A. Fujiwara, T. Kodama, K. Kikuchi, H. Imahori, Y. Misaki, S. Suzuki and Y. Achiba, *Appl. Phys. A: Mater. Sci. Process.*, 2002, **74**, 349–354.
56 B. W. Smith, R. M. Russo, S. B. Chikkannanavar and D. E. Luzzi, *J. Appl. Phys.*, 2002, **91**, 9333–9340.
57 Y. Maniwa, H. Kataura, M. Abe, A. Fujiwara, R. Fujiwara, H. Kira, H. Tou, S. Suzuki, Y. Achiba, E. Nishibori,

M. Takata, M. Sakata and H. Suematsu, *J. Phys. Soc. Jpn.*, 2003, **72**, 45–48.
58 T. W. Chamberlain, J. C. Meyer, J. Biskupek, J. Leschner, A. Santana, N. A. Besley, E. Bichoutskaia, U. Kaiser and A. N. Khlobystov, *Nat. Chem.*, 2011, **3**, 732–737.
59 E. Nakamura, M. Koshino, T. Saito, Y. Niimi, K. Suenaga and Y. Matsuo, *J. Am. Chem. Soc.*, 2011, **133**, 14151–14153.
60 L. Zhu, T. Zhang, M. Yi and J. Wang, *J. Phys. Chem. A*, 2010, **114**, 9398–9403.
61 H. Ulbricht, G. Moos and T. Hertel, *Phys. Rev. Lett.*, 2003, **90**, 095501.
62 T. Yasuike and S. Yabushita, *J. Phys. Chem. A*, 1999, **103**, 4533–4542.
63 L. Wang, Z. Cai, J. Wang, J. Lu, G. Luo, L. Lai, J. Zhou, Z. Qin, D. Yu, G. Li, W. N. Mei and S. Sanvito, *Nano Lett.*, 2008, **8**, 3640–3644.
64 V. V. Maslyuk, A. Bagrets, V. Meded, A. Arnold, F. Evers, M. Brandbyge, T. Bredow and I. Mertig, *Phys. Rev. Lett.*, 2006, **97**, 097201.
65 L. Shen, S.-W. Yang, M.-F. Ng, V. Ligatchev, L. Zhou and Y. Feng, *J. Am. Chem. Soc.*, 2008, **130**, 13956–13960.
66 L. Ge, B. Montanari, J. H. Jefferson, D. G. Pettifor, N. M. Harrison and G. A. D. Briggs, *Phys. Rev. B: Condens. Matter Mater. Phys.*, 2008, **77**, 235416.
67 J. M. Soler, J. Artacho, J. D. Gale, A. García, J. Junquera, P. Ordejón and D. J. Sánchez-Portal, *J. Phys.: Condens. Matter*, 2002, **14**, 2745–2779.
68 J. P. Perdew and A. Zunger, *Phys. Rev. B: Condens. Matter Mater. Phys.*, 1981, **23**, 5048–5079.
69 N. Troullier and J. L. Martins, *Phys. Rev. B: Condens. Matter Mater. Phys.*, 1991, **43**, 1993–2006.
70 N. Troullier and J. L. Martins, *Phys. Rev. B: Condens. Matter Mater. Phys.*, 1991, **43**, 8861–8869.
71 M. Brandbyge, J. Mozos, P. Ordejón, J. Taylor and K. Stokbro, *Phys. Rev. B: Condens. Matter Mater. Phys.*, 2002, **65**, 165401.
72 S. L. Dudarev, G. A. Botton, S. Y. Savrasov, C. J. Humphreys and A. P. Sutton, *Phys. Rev. B: Condens. Matter Mater. Phys.*, 1998, **57**, 1505–1509.
73 X. Zhang, J. L. Wang and X. C. Zeng, *J. Phys. Chem. A*, 2009, **113**, 5406–5413.
74 X. Zhang, J. L. Wang, Y. Gao and X. C. Zeng, *ACS Nano*, 2009, **3**, 537–545.

Electronic Supplementary Material (ESI) for Journal of Materials Chemistry C

Carbon nanotube and boron nitride nanotube hosted C_{60}-V nanopeapods

Guiling Zhang,[1,3] Rulong Zhou,[2,3] Xiao Cheng Zeng[3,*]

[1]*Key Laboratory of Green Chemical Engineering and Technology of College of Heilongjiang Province, College of Chemical and Environmental Engineering, Harbin University of Science and Technology, Harbin 150040, China*

[2]*School of Science and Engineering of Materials, Hefei University of Technology, Hefei, Anhui, 230009, China*

[3]*Department of Chemistry, University of Nebraska-Lincoln, Lincoln, NE 68588*

Table S1. Calculation Results Per Supercell of **1a**-**1h** and **2a**-**2h** Peapods in the Antiferromagnetic (AFM) and Ferromagnetic (FM) States: Total energy (E), Energy Difference between the FM and AFM States ($\Delta E_{FM\text{-}AFM}$), Total Magnetic Moment (S), and Reaction Energy (ΔE_r). The Data for V-free C_{60}@CNT and C_{60}@BNNT are Listed for Comparison. Abbreviation: hfh refers to hexagon-facing-haxagon, and pfh refers to pentagon-facing-hexagon.

Peapods	E_{AFM} (eV)	E_{FM} (eV)	$\Delta E_{FM\text{-}AFM}$ (meV)	S_{AFM}/S_{FM} (μ_B)	$\Delta E_{r,AFM}/\Delta E_{r,FM}$ (eV)
SIESTA Calculation Results					
Multi-Pod Structures					
1a (η^6-$C_{60}V$)@CNT	-68839.00998	-68838.90292	107.06	0.0/2.0	-18.54/-18.44
2a (η^6-$C_{60}V$)@BNNT	-77230.88150	-77230.80118	80.32	0.0/2.2	-18.44/-18.36
1b (η^5-$C_{60}H_{10}V$)@CNT	-69170.70640	-69170.70278	3.62	0.0/6.0	-26.68/-26.68
2b (η^5-$C_{60}H_{10}V$)@BNNT	-77562.45878	-77562.45640	2.38	0.0/6.0	-26.46/-26.46
1c (η^5-$C_{60}V$)@CNT	-68837.31546	-68837.13664	178.82	0.0/6.8	-16.86/-16.68
2c (η^5-$C_{60}V$)@BNNT	-77229.69066	-77229.38332	307.34	0.0/6.8	-17.26/-16.94
1d (η^6-$C_{60}H_{12}V$)@CNT	-69227.52458	-69227.50888	15.7	0.0/2.0	-21.22/-21.20
2d (η^6-$C_{60}H_{12}V$)@BNNT	-77618.17744	-77618.16876	8.68	0.0/2.0	-19.90/-19.88
V-Side-Binding Structures					
1e ($C_{60}V$)@CNT(hfh) *cis*	-68837.85062	-68837.93756	86.94	0.0/2.0	-
2e ($C_{60}V$)@BNNT(hfh) *cis*	-77228.04736	-77228.07838	31.02	0.0/2.0	-
1f ($C_{60}V$)@CNT(hfh) *trans*	-68837.94528	-68837.97022	24.94	0.0/2.0	-
2f ($C_{60}V$)@BNNT(hfh) *trans*	-77228.21776	-77228.19430	-23.46	0.0/2.0	-
1g ($C_{60}V$)@CNT(pfh) *cis*	-68837.65960	-68837.52740	-132.20	1.0/9.0	-
2g ($C_{60}V$)@BNNT(pfh) *cis*	-77227.83082	-77227.82054	-10.28	0.0/10.0	-
1h ($C_{60}V$)@CNT(pfh) *trans*	-68837.65586	-68837.65472	-1.14	0.0/10.0	-
2h ($C_{60}V$)@BNNT(pfh) *trans*	-77228.05754	-77228.04272	-14.82	0.0/10.0	-
V-free Species					
C_{60}@CNT (pfp)	-34056.85783	-	-	0.0	-6.92
C_{60}@CNT (hfh)	-34056.77958	-	-	0.0	-6.76
C_{60}@BNNT(pfp)	-38252.77402	-	-	0.0	-6.78
C_{60}@BNNT(hfh)	-38252.71239	-	-	0.0	-6.66
VASP Calculation Results					
1a (η^6-$C_{60}V$)@CNT	-4015.6230	-4015.5856	37.4	0.0/2.0	-
2a (η^6-$C_{60}V$)@BNNT	-3878.6422	-3878.5124	129.8	0.0/2.0	-
1b (η^5-$C_{60}H_{10}V$)@CNT	-4095.1300	-4095.1304	0.4	0.0/6.0	-
2b (η^5-$C_{60}H_{10}V$)@BNNT	-3958.8224	-3958.8206	1.8	0.0/6.0	-
1c (η^5-$C_{60}V$)@CNT	-4013.5262	-4013.4626	63.6	0.0/6.8	-
2c (η^5-$C_{60}V$)@BNNT	-3877.4412	-3877.2968	144.4	0.0/7.0	-
1d (η^6-$C_{60}H_{12}V$)@CNT	-4101.5286	-4101.4628	65.8	0.0/2.0	-
2d (η^6-$C_{60}H_{12}V$)@BNNT	-3964.2970	-3964.2896	7.4	0.0/2.0	-

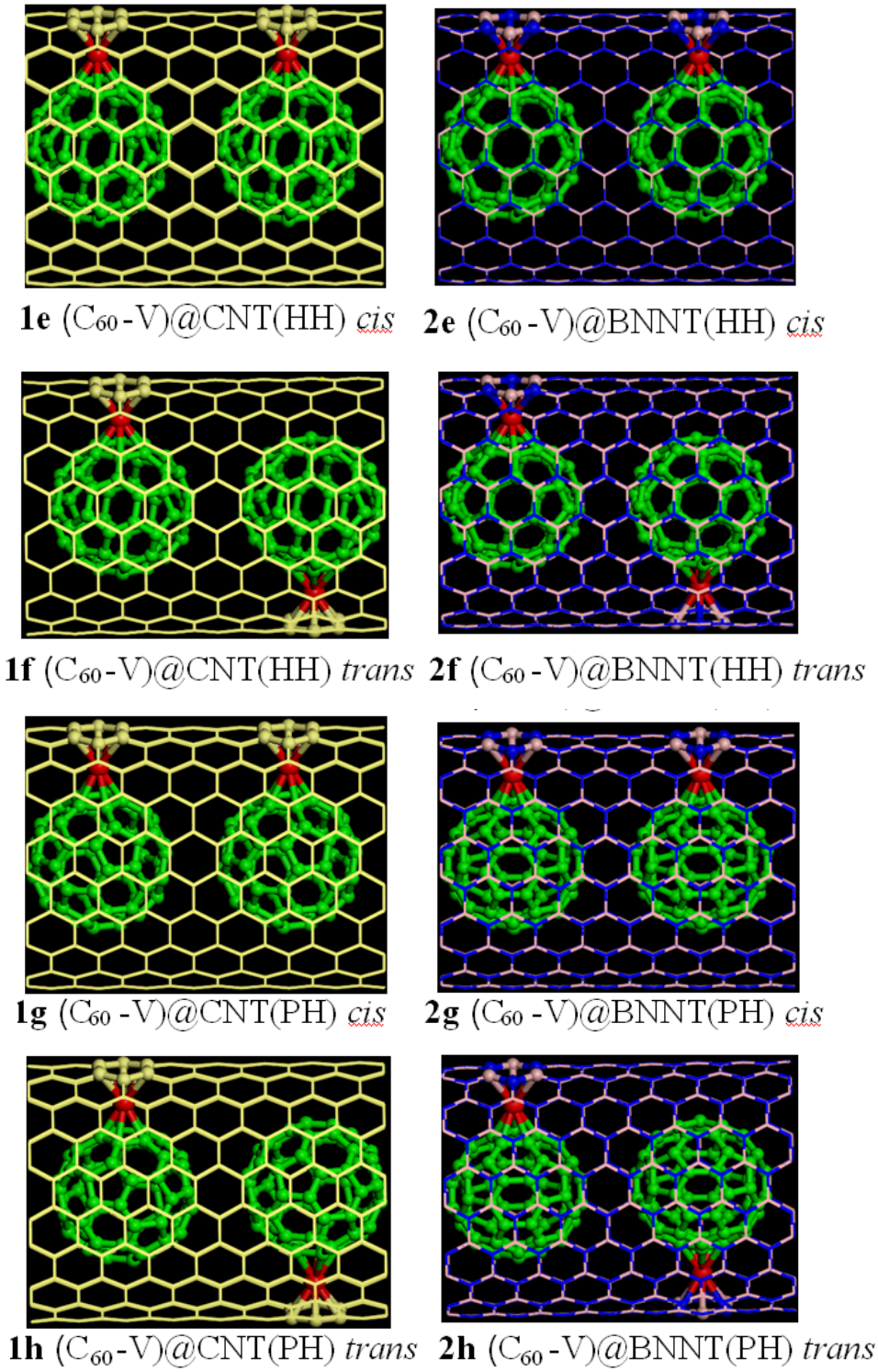

Figure S1. Optimized side-V-binding structures of **1e-1h** and **2e-2h** peapods. We denote a pVh structure if the C_{60} uses the pentagon and the tube uses the pentagon to coordinate with the V atom and a HH structure if both C_{60} and tube use the hexagon.

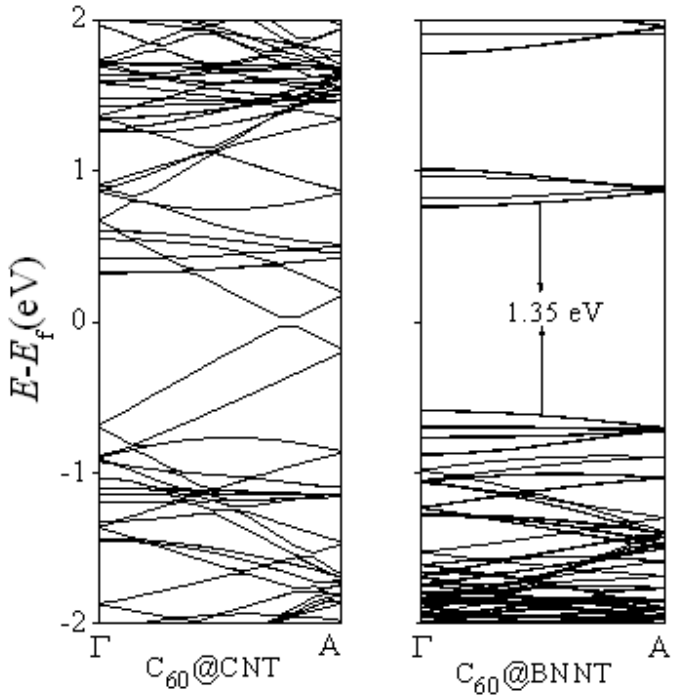

Figure S2. Computed band structures of C_{60}@CNT and C_{60}@BNNT peapods.